A visão sistêmica e integrada das engenharias e sua integração com a sociedade

2

Carlos Augusto Zilli
(Organizador)

Atena
Editora
Ano 2021

A visão sistêmica e integrada das engenharias e sua integração com a sociedade

2

Carlos Augusto Zilli
(Organizador)

Atena
Editora
Ano 2021

Editora chefe
Profª Drª Antonella Carvalho de Oliveira
Assistentes editoriais
Natalia Oliveira
Flávia Roberta Barão
Bibliotecária
Janaina Ramos
Projeto gráfico
Natália Sandrini de Azevedo
Camila Alves de Cremo
Luiza Alves Batista
Maria Alice Pinheiro
Imagens da capa
iStock
Edição de arte
Luiza Alves Batista
Revisão
Os autores

Atena Editora
Ano 2021

Ciências Exatas e da Terra e Engenharias

Atena Editora
Ano 2021

Ciências Exatas e da Terra e Engenharias

Atena Editora
Ano 2021

Ciências Exatas e da Terra e Engenharias

A visão sistêmica e integrada das engenharias e sua integração com a sociedade 2

Diagramação: Camila Alves de Cremo
Correção: Flávia Roberta Barão
Indexação: Gabriel Motomu Teshima
Revisão: Os autores
Organizador: Carlos Augusto Zilli.

Dados Internacionais de Catalogação na Publicação (CIP)

V822 A visão sistêmica e integrada das engenharias e sua integração com a sociedade 2 / Organizador Carlos Augusto Zilli. – Ponta Grossa - PR: Atena, 2021.

Formato: PDF
Requisitos de sistema: Adobe Acrobat Reader
Modo de acesso: World Wide Web
Inclui bibliografia
ISBN 978-65-5983-399-3
DOI: https://doi.org/10.22533/at.ed.993211308

1. Engenharia. I. Zilli, Carlos Augusto (Organizador). II. Título.

CDD 620

Elaborado por Bibliotecária Janaina Ramos – CRB-8/9166

Atena Editora
Ponta Grossa – Paraná – Brasil
Telefone: +55 (42) 3323-5493
www.atenaeditora.com.br
contato@atenaeditora.com.br

Atena Editora
Ano 2021

Ciências Exatas e da Terra e Engenharias

DECLARAÇÃO DOS AUTORES

Os autores desta obra: 1. Atestam não possuir qualquer interesse comercial que constitua um conflito de interesses em relação ao artigo científico publicado; 2. Declaram que participaram ativamente da construção dos respectivos manuscritos, preferencialmente na: a) Concepção do estudo, e/ou aquisição de dados, e/ou análise e interpretação de dados; b) Elaboração do artigo ou revisão com vistas a tornar o material intelectualmente relevante; c) Aprovação final do manuscrito para submissão.; 3. Certificam que os artigos científicos publicados estão completamente isentos de dados e/ou resultados fraudulentos; 4. Confirmam a citação e a referência correta de todos os dados e de interpretações de dados de outras pesquisas; 5. Reconhecem terem informado todas as fontes de financiamento recebidas para a consecução da pesquisa; 6. Autorizam a edição da obra, que incluem os registros de ficha catalográfica, ISBN, DOI e demais indexadores, projeto visual e criação de capa, diagramação de miolo, assim como lançamento e divulgação da mesma conforme critérios da Atena Editora.

Atena Editora
Ano 2021

DECLARAÇÃO DA EDITORA

Ciências Exatas e da Terra e Engenharias

Atena Editora
Ano 2021

APRESENTAÇÃO

Esta obra, intitulada “A Visão Sistêmica e Integrada das Engenharias e sua Integração com a Sociedade”, em seu segundo volume, apresenta 22 capítulos que abordam pesquisas relevantes que fazem emergir esta visão completa e abrangente típica das engenharias, revelando de que forma ela pode se integrar à sociedade para solucionar os desafios que surgem mundo afora, trazendo pesquisas relacionados à fluxo de potência, prevenção de ansiedade, reconstrução anatômica, modelagem energética, otimização de vigas mistas, composição de séries dodecafônicas, ruídos, entre outras.

Desta forma, esta obra se mostra potencialmente disponível para contribuir com discussões e análises aprofundadas acerca de assuntos atuais e relevantes, servindo como base referencial para futuras investigações relacionadas às engenharias em suas mais diversas instâncias.

Deixo, aos autores dos capítulos, um agradecimento especial, e aos futuros leitores, anseio que esta obra sirva como fonte inspiradora e reflexiva.

Esta obra é indicada para os mais diversos leitores, tendo em vista que foi produzida por meio de linguagem fluída e abordagem prática, o que favorece a compreensão dos conceitos apresentados pelos mais diversos públicos, sendo indicada, em especial, aos amantes da área de engenharia.

Carlos Augusto Zilli

SUMÁRIO

CAPÍTULO 8

NUMERICAL ANALYSIS OF BLOCKAGE EFFECT ON AN INNOVATIVE VERTICAL TURBINE (VAACT)

Data de aceite: 02/08/2021
Data de submissão: 04/05/2021

Rodrigo Batista Soares
Laboratório de Ondas e Correntes (LOC-COPPE/UFRJ)
Rio de Janeiro – Rio de Janeiro
http://lattes.cnpq.br/1544254318741858

Antonio Carlos Fernandes
Laboratório de Ondas e Correntes (LOC-COPPE/UFRJ)
Rio de Janeiro – Rio de Janeiro
http://lattes.cnpq.br/9090850388628824

Joel Sena Sales Junior
Laboratório de Ondas e Correntes (LOC-COPPE/UFRJ)
Rio de Janeiro – Rio de Janeiro
http://lattes.cnpq.br/4302624540517267

ABSTRACT: This paper aims to investigate the blockage effect at Laboratory of Waves and Currents' test facility through bidimensional numerical model. Then, simulations were carried out in order to achieve how control volume width must affect a static flat plate model for determining hydrodynamic coefficients as function of blockage ratio. Firstly, the numerical model made in ANSYS®/Fluent (ANSYS Inc., 2021) has been studied to understand its sensitivity for the main input parameters. After getting a robust numerical model, it has been validated by comparing it to flat plate's experimental results reached in Fernandes and Rostami (2015), verifying whether there is agreement between both approaches. Concerning the analyses about different blockage ratios, the results have shown there is a straight relation among the hydrodynamic coefficients and that parameter, being possible to attain linear regressions in order to represent flat plate coefficients against blockage ratio in function of angle of attack.

KEYWORDS: Computational Fluid Dynamics (CFD), VAACT, Blockage Effect.

ANÁLISE NUMÉRICA DO EFEITO DE BLOQUEIO EM UMA TURBINA VERTICAL INOVADORA(VAACT)

RESUMO: Este artigo analisa a influência do efeito de bloqueio no Canal de Correntes do Laboratório de Ondas e Correntes (LOC-COPPE/UFRJ) através de modelo numérico bidimensional. Dessa forma, simulações foram realizadas obtendo a influência da largura do volume de controle em uma placa plana estática a fim de se determinar o comportamento de parâmetros de interesse em função da razão de bloqueio. Primeiramente, investigou-se o modelo numérico criado em ANSYS®/Fluent (ANSYS Inc., 2021) para estudar sua sensibilidade aos parâmetros de entrada das simulações. Após a criação de um modelo numérico robusto, validou-se a abordagem através de resultados experimentais para placa plana contidos em Fernandes e Rostami (2015) para se verificar a concordância entre os resultados experimentais e numéricos. O estudo da influência da razão de bloqueio sobre os coeficientes hidrodinâmicos do modelo mostrou que há uma relação de proporcionalidade entre esses adimensionais

cuja estimativa é feita a partir de regressões lineares em diferentes ângulos de ataque.

PALAVRAS-CHAVE: Mecânica dos Fluidos Computacional (CFD), VAACT, Efeito de Bloqueio.

1 I INTRODUCTION

This work aims to discuss about blockage effect influence on a static flat plate turbine subjected to uniform flow. From the literature, the control volume dimensions seem to affect the output parameters of both experimental and numerical models. Indeed, the velocity, pressure and vorticity fields have been significantly affected by model-flow interaction for different control volume widths, being it responsible for increasing the flow velocity whereas there is a pressure drop nearby the body on the control volume.

Then, this research is going to take the physical meaning regarding blockage effect on the flow as well as define the hydrodynamic coefficients of a bidimensional flat plate subjected to a uniform flow through numerical model made in ANSYS®/Fluent. As result, it expects to get mathematical relations in order to model the relation among the hydrodynamic loads of that model as function of blockage ratio for different angles of attack between flow and flat plate model.

Furthermore, a detailed description about the device Vertical Axis Autorotation Current Turbine (VAACT) has been brought in this paper. The VAACT turbine is an ultra-low-head technology which has been capable of harvesting energy from hydrokinetic sources with low Reynolds numbers () and high efficiencies. Thus, its explanations are requested on this work just because blockage effect analysis is a branch from many investigations carried out for implementing that concept with reasonable technical and economic feasibility.

2 I VERTICAL AXIS AUTOROTATION CURRENT TURBINE

The VAACT turbine consists in a vertical axis device for harvesting energy from low and moderate Reynolds numbers. Since 2009, numerical and experimental investigations have been carried out for understanding its behaviour based on hydrodynamic phenomena surrounding that rotor. Concerning turbine's motions, it can perform two main phenomena: fluttering and autorotation. As result of flow passing through turbine model, the fluttering means an oscillatory motion which the rotor does around itself whereas the autorotation is a self-rotation motion managed by the extra moment of inertia over the model.

Moreover, this model presents two main shapes. The first one is called flat plate whereas the second shape is the flapped plate. The Figure 1 displays both turbine models which have been tested in LOC's current flume. According to Rostami and Fernandes (2015), flapped model may have flap angles either 27º or 55º.

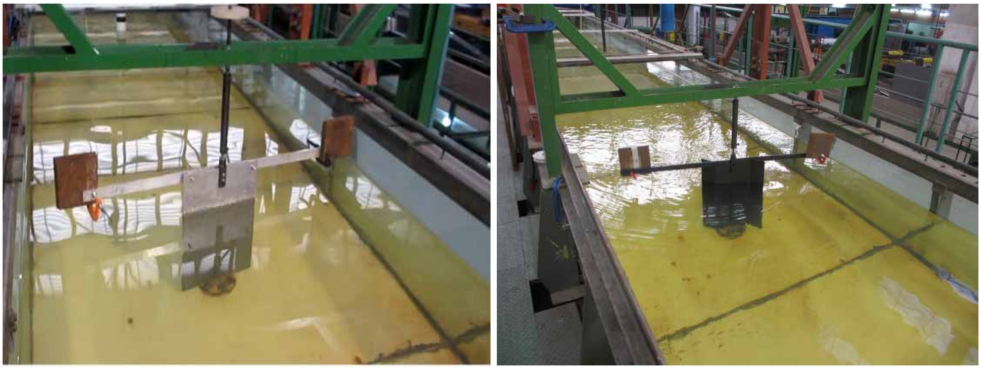

(a) Flat plate turbine (b) Flapped plate turbine

Figure 1 – VAACT turbine - possible shapes (Rostami, 2015).

Fernandes and Rostami (2015) have employed experimental analysis for estimating the efficiency curves of a flat plate turbine submitted to uniform flow. Those experiments were made at LOC-COPPE/URFJ to different Reynolds numbers and dimensionless moment of inertia. Then, the results for rotating flat plate have shown its maximum efficiency is about 7% when is in the range 0.5-0.6 and the Reynolds number is about 59,800.

Rostami and Fernandes (2015) carried out experiments to verify the maximum efficiency of a flapped plate model doing autorotation motion in analogous conditions to Fernandes and Rostami (2015). Those experiments have adopted a turbine with 27º degrees flap angle, leading to an efficiency peak about 33% whether I^* is between 0.6 and 0.7 as well as Re is 21,200.

Rostami and Fernandes (2017) have compared both experimental and numerical results from VAACT motions submitted to uniform flow. In addition to the excellent agreement between those models, the work has been suggesting the flat plate model must achieve a maximum efficiency of 19% for a flat plate turbine performing fluttering phenomenon.

Rostami and Fernandes (2018) have checked turbine's performance through far-field method for modelling both fluttering and autorotation phenomena. That method is a more robust model to estimate rotor's parameters, having taken into account the exciting moment due to vortex shedding by the rotor. In fact, the vortex contribution on the far-field has been allowing them achieving a good matching between numerical and experimental results in comparison to Rostami and Fernandes (2017).

Soares et al. (2020) have performed numerical studies with two-dimensional turbines to estimate the hydrodynamic coefficients as function of the Reynolds number and different angles of attack. The verification of those results has shown there is no significant dependence of interest parameters to as they have been almost constant on the range 43,000-117,000.

Soares et al. (2021) numerically analysed blockage effect influence in determining the lift and drag coefficients of a flat plate turbine. Then, they have been figuring out that increasing blockage ratio implies in increasing the parameters values so that there might be a straight relation among those hydrodynamic loads and the blockage ratio.

3 I BLOCKAGE EFFECT

The blockage effect represents the influence from control volume walls on the flow. According to Ryi et al. (2015), if it is greater than 10%, the effect should not be neglected on the analyses. Thus, the results achieved may need corrections for accounting how blockage effect affects the flow due to the distance between walls on the control volume.

Ryi et al. (2015) have suggested there are studies establishing corrections to account blockage effect on the parameters of system. Among them, Glauert (1933) was pioneer on correcting coefficients because of blockage effect in wind tunnel to evaluate a propeller using actuator disk technique.

On the other hand, Ryi et al. (2015) still mentions that Fitzgerald (2007) has further utilized blockage corrections in order to study propellers in the closed-circuit condition installed at Glenn L. Martin Wind Tunnel (GLMN), in Maryland. Adamarola and Krogstad (2011) also have added to blockage effect studies as they had been analysing the performance of a rotor with some wake states.

According to Ross (2010), there might be three blockage effect types acting on the flow: solid, wake and total blockage effects. The solid blockage arises due to a reduction in the test section area after placing a body on the flow. Thus, it induces a local increasing on velocity as well as a pressure drop close to body location.

Besides that, the wake blockage effect happens if there is wake formation behind the body. That means both pressure and velocity intensities depend on body shape and wake intensity due to fluid-to-body interaction. Nevertheless, those fields keep similar behaviour regarding solid blockage effect – i.e., the pressure drops whereas the velocity becomes larger. Finally, the total blockage effect consists on a superposition from both solid and wake blockage effects.

4 I DIMENSIONAL ANALYSIS

The blockage phenomenon considers that drag (C_D) and lift (C_L) coefficients from flat plate model are mainly affected by the blockage ratio (ϵ_{be}) on the control volume and its angle of attack (θ). Thus, Equation (1) gets this relation:

$$\{C_L, C_D\} = f(\epsilon_{be}, \theta) \tag{1}$$

The blockage ratio is calculated using the ratio between the turbine chord (c) and control volume width (w). On the other hand, lift and drag coefficients depend on their respective forces and flow velocity. The Equations (2)-(4) illustrate the expressions to ϵ_{be}, C_L and C_D:

$$\epsilon_{be} = \frac{c}{w} \tag{2}$$

$$C_L = \frac{L}{\frac{1}{2}\rho A U_\infty^2} \tag{3}$$

$$C_D = \frac{D}{\frac{1}{2}\rho A U_\infty^2} \tag{4}$$

Where U_∞ is the flow velocity, ρ is the fluid density, is the wetted area of model; *L* and *D* are lift and drag forces, respectively. Two-dimensional models usually take that area assuming a unitary plate height. The above expressions intend to ratify the importance of analysing both lift and drag coefficients against angle of attack and blockage ratio. Hence, the following sections are going to bring numerical results of $\{C_L, C_D\}$ x $\{\epsilon_{be}, \theta\}$.

5 | NUMERICAL MODEL

5.1 Geometric model and boundary conditions

The two-dimensional geometric model was made by using CAD tools from ANSYS®. That geometry presents two main surfaces: turbine and fluid domain. By the way, the plate follows the same dimensions from LOC's flat plate model - i.e., it has 0.3 m chord and 5 mm thickness (Fernandes and Rostami, 2015). As the model is two-dimensional, the flat plate model does not have height but the software makes a unitary height only for calculating its wetted area, which is about 0.61 m². The Figure 2 displays the boundary conditions which have been employed on the simulations. Thus, the flat plate and domain walls receive wall boundary condition (no-slip); the inlet and outlet are going to get velocity and pressure boundary conditions, respectively. Moreover, the pressure gauge (P_{gauge}) on the outlet has been addressed as zero because that means the pressure in both inlet and outlet are equal to the atmospheric pressure.

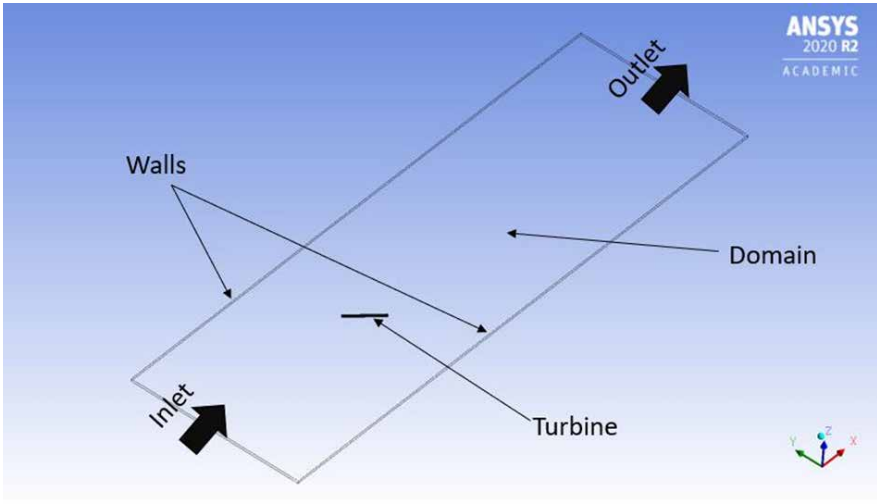

Figure 2 - Domain and its boundaries.

Regarding the velocity at the inlet, it has been about 0.39 m/s (Re = 177,000) in the whole simulations just because previous investigations have shown the hydrodynamic coefficients do not significantly change with Reynolds number (Soares et al., 2020), besides existing experimental data for model validation in that *Re* value which ratify that behaviour as well (Fernandes and Rostami, 2015).

5.2 Domain independence

The domain sensitivity study has been performed to four domain lengths with same width, where it is about 1.4 meters because LOC's current flume having that dimension. In fact, LOC's test facility is where the flat plate model utilized for validating this method has been tested. Thus, Table 1 leads to main lengths used on the analysis.

Domain	Width	Upstream	Downstream	Total
1	1.4 m	1.5 m	3.0 m	4.5 m
2	1.4 m	3.0 m	6.0 m	9.0 m
3	1.4 m	6.0 m	9.0 m	15.0 m
4	1.4 m	9.0 m	12.0 m	21.0 m

Table 1 - Domain dimensions on the sensitivity study.

From the above table, the shorter domain has 4.5 meters length whereas the largest one achieves 21 meters length. In addition, the domain independence test is done at 90 degrees angle of attack. That means the drag coefficient is going to be the maximum whereas the lift coefficient is about zero. Hence, this sensitivity study has only taken drag coefficient into account. The Figure 3(a) brings the results to domain sensitivity study at θ=90º:

It is noticed the results present good agreement, even though they can significantly differ regarding their domain lengths. Indeed, the larger discrepancy on the approach is about 5% between the first and fourth domains. Note that is not a very significant error on the analysis. Then, this paper has proposed choosing domain 1 just because its simulations require less computational efforts from the computer.

5.3 Grid independence

The grid sensitivity study has been carried out at 45 degrees angle of attack, considering four mesh types which are called: coarse, medium, fine and very fine. The cells on the domain have a general element size of 0.02 meters and both structured and unstructured approaches have been employed for making the grid.

Then, the grid sensitivity study may get a comparison among output parameters for the whole grids tested in this stage. As Figure 3(b) have shown, the grid seems to converge from fine mesh just because the discrepancy among the output values perhaps decreases as number of elements on the grid becomes greater.

Indeed, the figure gives C_D has 0.7% discrepancy when the grid is compared between fine and very fine mesh. On the other hand, the Figure 3(c) displays that both grids have good Y^+ values nearby domain and turbine walls due to that value is less than 5 (y+ < 5). That means the interaction of fluid to walls has been modelled properly in those meshes.

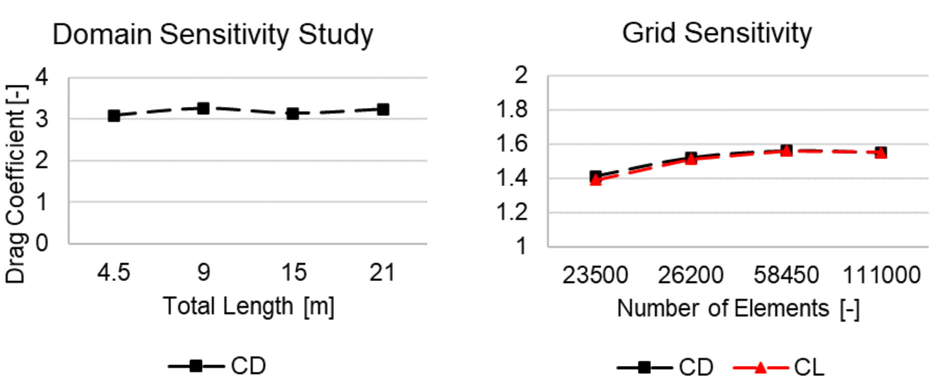

(a) Convergence of C_D – domain sensitivity (b) Convergence of C_D and C_L – grid sensitivity

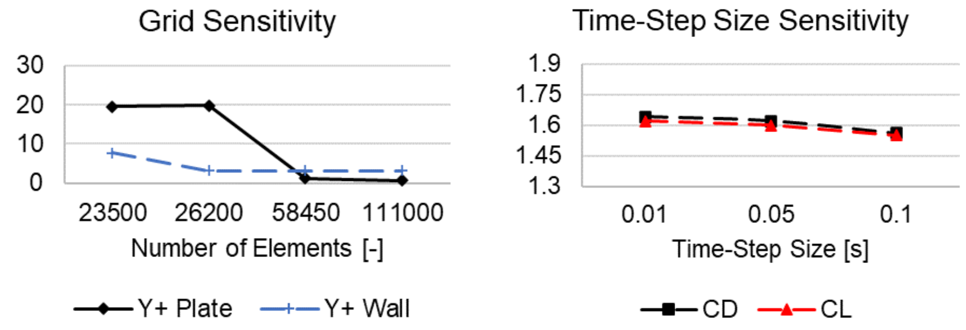

(c) Convergence of Y^+ – grid sensitivity (d) Convergence of C_D and C_L – time-step size sensitivity

Figure 3 – Results from the sensitivity studies.

Hence, those analyses allow to conclude the simulations should go ahead utilizing very fine mesh not only because the output parameters have converged but they have also presented reasonable Y^+ values on turbine and domain walls. The Figure 4 provides further details about very fine mesh which has been using unstructured mesh to improve grid resolution close to flat plate model and its wake as well as a couple of layers aiming better capturing the gradients on walls and plate.

5.4 Time-step independence

Regarding the time-step sensitivity study, it has been accomplished at 45 degrees angle with the following time-step sizes: $\Delta t = 0.01s$, $\Delta t = 0.05s$ and $\Delta t = 0.10s$. As seen in Figure 3(d), there is good agreement between $\Delta t = 0.05s$ and $\Delta t = 0.01s$ results as the discrepancy of C_D reaches 1.2% for those time-step sizes. However, that value is about 4% between 0.05 s and 0.10 s.

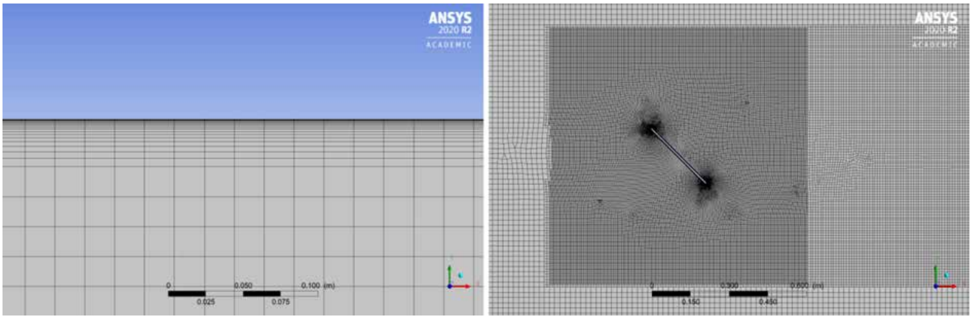

(b) Wall view (c) Grid nearby geometry

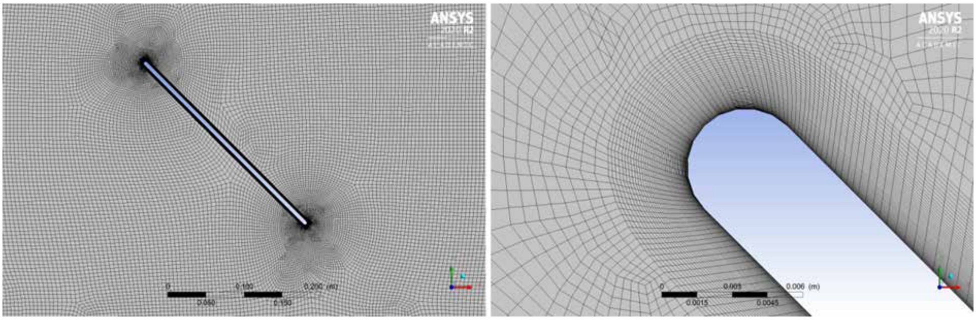

(d) Grid close to TEV and LEV

(e) Inflation on flat plate

Figure 4 – Very fine mesh assembly.

5.5 Turbulence model

This section brings results for simulations with the following turbulence models: Shear-Stress Transport (SST) k-ω and Detached Eddy Simulation (DES) SST Realizable k-ϵ. These simulations have been performed at 90 degrees angle of attack to the static flat plate model. Their main settings are shown in Table 2.

From the table, the whole models get SIMPLE scheme for pressure-velocity; the gradient uses least square cell based; the pressure is solved with second order scheme; the momentum has been using second order upwind for SST k-ω and bounded-central differencing for DES model; the turbulence kinetic energy (k), rate of dissipation of turbulent kinetic energy (ϵ), and specific rate of dissipation of the turbulence kinetic energy (ω) are solved with second order upwind scheme; all the cases use bounded second order implicit scheme for resolving the transient formulation.

Property	**SST k-ω**	**DES Realizable k-ϵ**
Pressure-Velocity Coupling	SIMPLE	
Gradient	Least Squares Cell Based	
Pressure	Second Order	
Momentum	Second Order Upwind	Bounded-Central Differencing
k	Second Order Upwind	Second Order Upwind
ϵ	-	Second Order Upwind
ω	Second Order Upwind	-
Transient Formulation	Bounded Second Order Implicit	

Table 2 - Settings to turbulence models.

The Figure 5 illustrates the velocity u component surrounding the two-dimensional flat plate model to both turbulence models. These velocity fields likely suggest the SST k-ω model does not represent adequately the flow just because it has not been properly showing the vortex shedding behind the model as the post-processing image seems a steady simulation. However, the DES model provides a better understanding of wake as it clearly shows the vortices in all images.

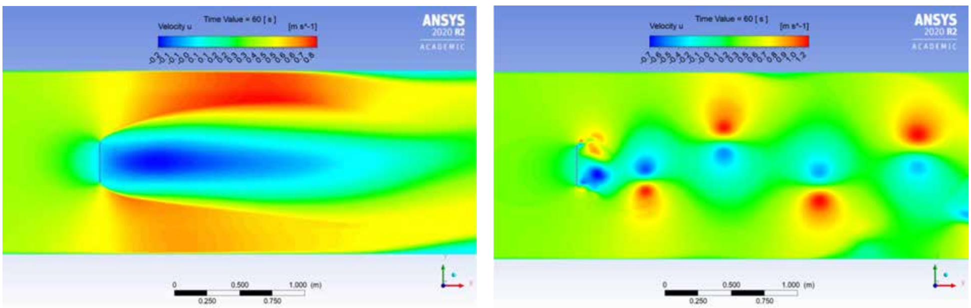

(a) SST k-

(b) DES Realizable k-

Figure 5 – Velocity u component.

5.6 Model validation

The numerical model can be validated through experimental results of a flat plate model obtained by Fernandes and Rostami (2015). They have been presenting their data for unbounded fluid. That means the output parameter already is corrected to a system without blockage effect. Then, the Table 3 compares both numerical and experimental results for drag coefficient in unbounded fluid:

Investigation	**C_D (Unbounded Fluid)**
Actual Study (DES Realizable k-ϵ)	1.83
Fernandes and Rostami (2015)	1.99

Table 3 – Model Validation.

From the table, there is good agreement between the numerical and experimental data, as they have a discrepancy of 8%.

6 I RESULTS AND DISCUSSIONS

The simulations have been carried out to control volumes with 5% up to 42% blockage ratio, meaning a channel width on the range 0.7 m to 6.0 m. Note that the experimental test facility has 21% blockage ratio. These relations are shown in Table 4:

Channel Width [m]	Blockage Ratio
6.0	5%
3.0	10%
2.0	15%
1.4	21%
0.7	42%

Table 4 – Blockage ratio on the simulations.

Then, the Figures 6 and 7 give the numerical data regarding lift and drag coefficients in function of blockage ratio. These results suggest there is a linear relation among C_L and C_D, and ϵ_{be} so that a linear regression may model the results for different angles of attack.

Moreover, the graphs have explained these coefficients do increase whether blockage ratio increase as well. That behaviour is clear in C_D x ϵ_{be} curves, where they indeed have a positive slope. Nevertheless, the lift coefficient also becomes greater but its slope is not very significant compared to drag coefficient curves. In addition, the lift curve has null value at 0 degrees because the plate model is parallel to the flow, meaning there is no lift force on the model.

Comparing the results for drag coefficient at 90 degrees angle of attack, the graph displays the blockage ratio may increase coefficient's magnitude about 11% if checking the data to unbounded fluid and 42% blockage ratio. That means the blockage corrections have to be done in order to achieve right data as the phenomenon can be significant on the analysis of a rigid body.

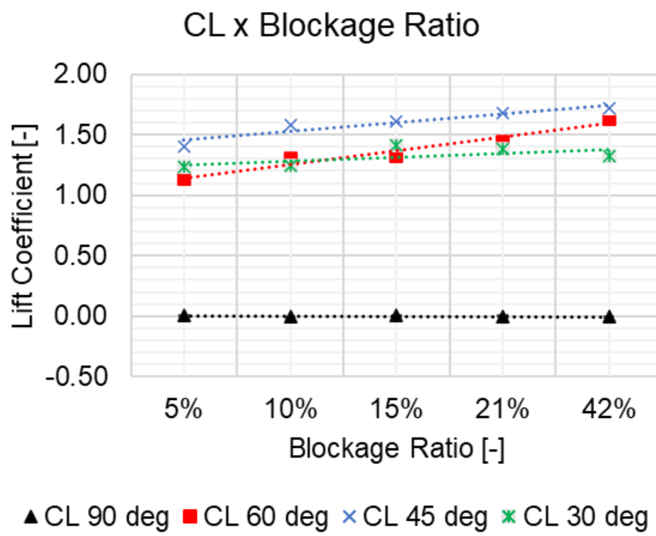

Figure 6 - Lift coefficient x Blockage effect.

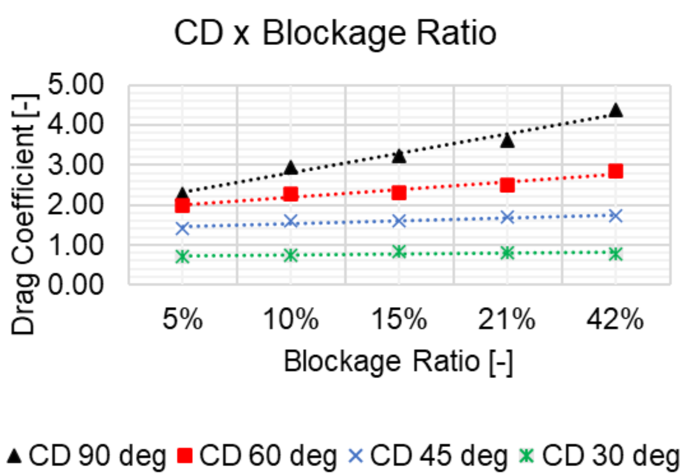

Figure 7 - Drag coefficient x Blockage effect.

The Table 5 provides the slope (*a*) and linear coefficient (*b*) of the regressions performed through the above figures. From the table, *b* can represent the hydrodynamic coefficient to unbounded fluid, when there is no blockage effect over the flat plate. Note that, there is good matching between numerical data and the regressions as the determination coefficient (R^2) is about one.

Although the figures perhaps show there might be good agreement to the results at 30 degrees angle of attack, the determination coefficients have provided that using it must require a few cations because the regressions does not seem to follow that behaviour.

Regressão: $y = a \cdot \epsilon_{be} + b$				
Coefficient	**Angle of Attack [deg]**	a [-]	b [-]	R^2[-]
C_L	30	0.0324	1.2199	0.41
	45	0.0717	1.3812	0.90
	60	0.1131	1.0281	0.94
	90	-0.0005	0.003	0.04
C_D	30	0.0185	0.7162	0.40
	45	0.0703	1.3658	0.89
	60	0.1946	1.7946	0.94
	90	0.4853	1.8374	0.98

Table 5 - Adjustment coefficients for linear regression.

Although the figures perhaps show there might be good agreement to the results at 30 degrees angle of attack, the determination coefficients have provided that using it must require a few cations because the regression does not seem to follow that behaviour.

The following figures illustrate the vorticity field and pressure coefficient for 5% and 42% blockage ratio at 45 degrees angle of attack. Thus, they have been clarifying the issue behind blockage ratio. As seen in Figure 8, a small distance between walls increases the interaction vortices-walls, becoming the wake more disturbed.

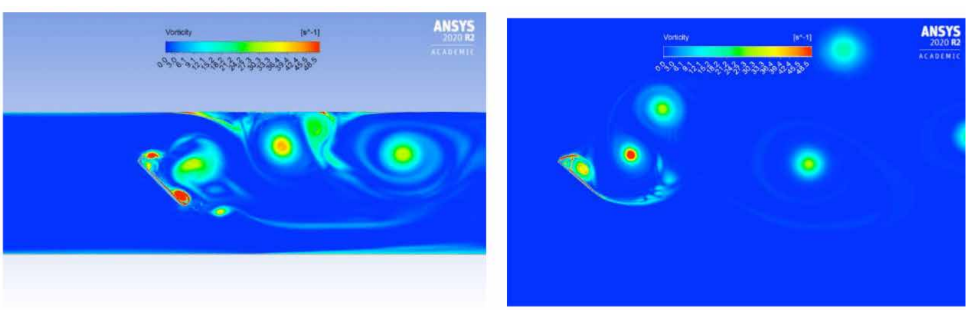

(a) $\epsilon_{be} = 42\%$ (b) $\epsilon_{be} = 5\%$

Figure 8 – Vorticity field for different blockage ratios.

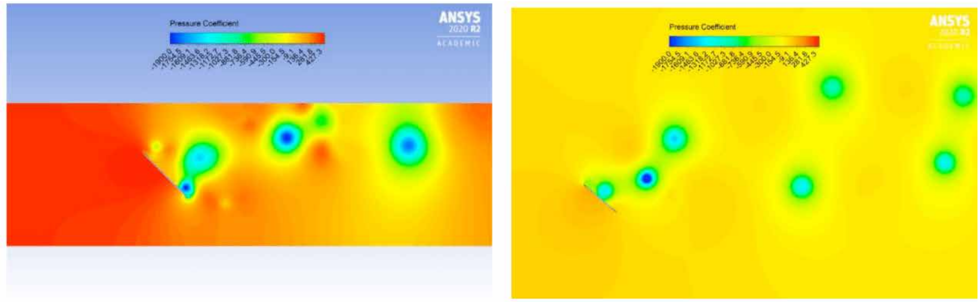

(a) $\epsilon_{be} = 42\%$ (b) $\epsilon_{be} = 5\%$

Figure 9 – Pressure coefficient for different blockage ratios.

On the other hand, that phenomenon is seen in Figure 9 as well. The pressure coefficient magnitude close to flat plate model with ϵ_{be} = 42% is higher than the case with ϵ_{be} = 5%. In fact, that happens just because the largest ϵ_{be} brings a stagnation point on the plate which increases the pressure coefficient nearby the model. Despite of having stagnation to ϵ_{be} = 5%, the fluid may freely flow on the control volume avoiding greater magnitudes.

7 I CONCLUSIONS

The paper has brought numerical results regarding the hydrodynamic coefficients of a two-dimensional flat plate model adopting a static approach. The numerical model made in CFD introduced the hypothesis and sensitivity tests which utilized to build a quite robust model. After studying the sensitivity of model, the gradients around the plate model and the hydrodynamic coefficients had been investigated for getting their magnitudes and allowing blockage corrections on a static flat plate. It is possible to conclude:

1. This study of blockage corrections has arisen with importance as it eventually is needed to ratify results;
2. From the sensitivity study of the model, it is possible to achieve the numerical configuration whose results are less sensitive;
3. The DES realizable k-ϵ model reaches acceptable output data for the applications developed throughout this study;
4. The CFD model allows a better understanding of the gradients around the flat plate with blockage phenomenon;
5. The study of different ϵ_{be} values has been allowing to get the C_D and C_L curves which enable making corrections of these values for different widths of the control volume.

REFERENCES

ADARAMOLA, M. S.; KROGSTAD, P. A. **Experimental investigation of wake effects on wind turbine performance**. Renewable Energy, v. 36, n. 8, p. 2078–2086, 2011. DOI: https://doi.org/10.1016/j.renene.2011.01.024.

ANSYS INC. **ANSYS Fluent Tutorial Guide**. Available in: http://www.ansys.com.

ROSTAMI, A. B.; FERNANDES, A. C. **Evaluation of dynamics of fluttering and autorotation of a rigid plate in a flow using far-field method**. Nonlinear Dynamics, v. 94, n. 3, p. 1619–1638, 2018. DOI: 10.1007/s11071-018-4445-1. Available in: https://doi.org/10.1007/s11071-018-4445-1.

FERNANDES, A. C.; ROSTAMI, A. B. **Hydrokinetic energy harvesting by an innovative vertical axis current turbine. Renewable Energy**, v. 81, p. 694–706, 2015. DOI: 10.1016/j.renene.2015.03.084. Available in: http://dx.doi.org/10.1016/j.renene.2015.03.084.

FITZGERALD, R. E. **Wind Tunnel Blockage Corrections for Propellers**. 2007. University of Maryland, 2007. Available in: http://hdl.handle.net/1903/7363.

GLAUERT, H. **Wind tunnel interference on wings, bodies and airscrews**. Available in: https://apps.dtic.mil/sti/pdfs/ADA953012.pdf.

ROSS, I. J. **Wind Tunnel Blockage Corrections**: An Application to Vertical Axis Wind Rotors. 2010. University of Dalton, 2010.

ROSTAMI, A. B. **Hydrokinetic Energy Harvesting by Autorotation of a Plate with Hinged Axis**. 2015. Universidade Federal do Rio de Janeiro, 2015.

ROSTAMI, A. B.; FERNANDES, A. C. **The effect of inertia and flap on autorotation applied for hydrokinetic energy harvesting**. Applied Energy, v. 143, p. 312–323, 2015. DOI: 10.1016/j.apenergy.2015.01.051. Available in: http://dx.doi.org/10.1016/j.apenergy.2015.01.051.

ROSTAMI, A. B.; FERNANDES, A. C. **From fluttering to autorotation bifurcation of a flat plate in a current**. Journal of the Brazilian Society of Mechanical Sciences and Engineering, v. 39, n. 11, p. 4769–4784, 2017. DOI: 10.1007/s40430-017-0912-8.

ROSTAMI, A. B.; MOBASHERAMINI, M.; FERNANDES, A. C. **Strouhal number of flat and flapped plates at moderate Reynolds number and different angles of attack: experimental data**. Acta Mechanica, v. 230, n. 1, p. 333–349, 2019. DOI: 10.1007/s00707-018-2292-2. Available in: https://doi.org/10.1007/s00707-018-2292-2.

RYI, J.; RHEE, W.; HWANG, U. C.; CHOI, J. S. **Blockage effect correction for a scaled wind turbine rotor by using wind tunnel test data**. Renewable Energy, v. 79, p. 227–235, 2015. DOI: https://doi.org/10.1016/j.renene.2014.11.057.

SOARES, R. B.; FERNANDES, A. C.; SALES JUNIOR, J. C. **Hydrodynamic Coefficients of the Vertical Axis Autorotation Current Turbine by CFD**. In: 8th International Congress on Waterborne Transportation, Shipbuilding and Offshore Constructions Proceedings 2020, Rio de Janeiro. DOI: 10.17648/sobena-2020-123074. Available in: https://proceedings.science/sobena-2020/papers/hydrodynamic-coefficients-of-the-vertical-axis-autorotation-current-turbine-by-cfd.

SOARES, R. B.; FERNANDES, A. C.; SALES JUNIOR, J. C. **Estudo do Efeito de Bloqueio em Placa Plana através de Computational Fluid Dynamics**. In: Anais da Jornada Giulio Massarani de Iniciação Científica, Tecnológica, Artística e Cultural. 2021, Rio de Janeiro. Rio de Janeiro Available in: https// www.even3.com.br.

ÍNDICE REMISSIVO

A

W

A visão sistêmica e integrada das engenharias e sua integração com a sociedade

2

www.atenaeditora.com.br
contato@atenaeditora.com.br
@atenaeditora
www.facebook.com/atenaeditora.com.br

Atena Editora
Ano 2021

A visão sistêmica e integrada das engenharias e sua integração com a sociedade

2

www.atenaeditora.com.br
contato@atenaeditora.com.br
@atenaeditora
www.facebook.com/atenaeditora.com.br

Atena Editora
Ano 2021